Journal of the Ceramic Society of Japan 124 [10] 1042-1045 2016 Full paper

UV Raman spectroscopy of segregated carbon in silicon oxycarbides

Felix ROTH, Philipp WALESKA,* Christian HESS,* Emanuel IONESCU† and Norbert NICOLOSO††

Institut für Material- und Geowissenschaften, Technische Universität Darmstadt, Jovanka-Bontschits-Str. 2, 64287 Darmstadt, Germany
***Eduard-Zintl-Institut für Anorganische und Physikalische Chemie, Technische Universität Darmstadt, Alarich-Weiss-Str. 8, 64287 Darmstadt, Germany**

Polymer-derived silicon oxycarbides exhibiting ≤1 and 10 vol.% of segregated carbon finely dispersed within a glassy $Si_xO_yC_z$ matrix have been investigated by UV Raman spectroscopy using a laser excitation of 4.8 eV ($\lambda = 256.7$ nm). Carbon exists as amorphous sp^2–sp^3 bonded component in SiOC/C (≤1 vol.%) pyrolyzed at 1100°C in H_2, including C–C single bonds, polymeric chains and small polycyclic aromatic hydrocarbons (PAHs). The formation of nanocrystalline carbon at T > 1400°C is seen in the Raman spectra of SiOC/C (≤1 vol.%) and SiOC/C (10 vol.%) by the appearance of the G band of graphite. Tempering at 1600°C increases the degree of order within the carbon phase. However, the slight narrowing of the G peak with processing temperature (by about 5%) indicates still not well-crystallized carbon: the Raman results can be best explained by turbostratic carbon (with a lateral size L_a of ≈2 nm) and do not support the model description in literature as a network of single layer graphene.

Key-words : UV Raman spectroscopy, Carbon, Graphite, Graphene, Nanocomposites, Polymer-derived ceramics

[Received April 27, 2016; Accepted May 21, 2016]

1. Introduction

Polymer-derived ceramics possess a variety of interesting properties like outstanding thermal stability against decomposition and crystallization,[1)–3)] excellent high-temperature creep resistance,[4),5)] piezoresistivity at ambient as well as high temperature,[6)] high reversible capacity concerning lithium-ion uptake and release[7)] and electromagnetic shielding[8)] which all rely on the presence of a segregated carbon phase randomly distributed within a glassy matrix.

Two types of carbons are present in silicon oxycarbides (SiOC): sp^3-hybridized, tetrahedrally bonded carbon within SiO_mC_{4-m} ($1 < m < 4$) structural units and a segregated carbon phase ("free carbon"), which is generated in situ upon the thermolysis of the organic substituents bonded to silicon in the polysiloxane precursor. Several studies indicate that the generation of the segregated carbon phase begins at temperatures as low as 500–800°C.[9)–11)] According to Monthioux et al. carbon starts to segregate as polycyclic aromatic hydrocarbons (PAHs) with lateral sizes of ≈1 nm.[12)] Dehydrogenation and edge-to-edge-linkage of neighboring PAHs lead to the formation of larger graphitic clusters within the silicon oxycarbide matrix.

Raman spectroscopy is a powerful and non-destructive technique, which allows for assessing lattice dynamics and vibrational spectroscopy of carbon-based materials such as amorphous carbon,[13),14)] carbon nanotubes,[15)–17)] graphene,[18),19)] graphite[20),21)] and diamand like carbon (DLC) materials.[22),23)] It is very sensitive to the s-p hybridization state of carbon and thus provides valuable information about the nano/microstructure and the degree of ordering of the material. The Raman spectrum of, e.g., diamond shows a single peak at 1333 cm^{-1} due to the tetrahedral sp^3-bonds, whereas sp^2-bonded graphite exhibits a peak at 1580 cm^{-1} assigned to the E_{2g} vibration (G mode). In case of structurally disordered graphite, the D mode with A_{1g} symmetry appears at 1380 cm^{-1} together with the G mode. Additional modes can be present in disordered carbon such as the ν_3- and ν_1-mode (1180 and 1520 cm^{-1}) due to polyolefinic chains and the G mode of amorphous carbon down-shifted to ≈1500 cm^{-1}, respectively. Visible Raman spectroscopy is far more sensitive to sp^2-sites than to sp^3-sites, making it hard to investigate the latter.[24),25)] With its higher photon energy of 4.8 eV, UV Raman spectroscopy excites both the π- and the σ-states allowing to probe sp^3 sites. We therefore applied UV Raman spectroscopy to gain more detailed insight into the different hybridization states of carbon in SiOC ceramics and their changes with temperature and concentration. As shown in the following, the ordering of carbon gradually increases with temperature and initial carbon concentration, ultimately leading to sp^2-bonded turbostratic graphite distributed within the glassy $Si_xO_yC_z$ matrix.

2. Experimental

Silicon oxycarbide (SiOC/C) containing 10 vol.% segregated carbon was prepared from a commercially available poly(methyl)silsesquioxane (PMS MK, Wacker AG, Munich, Germany), which was cross-linked at 250°C, pyrolyzed at 1100°C for 2 h under Argon and subsequently ball-milled and sieved to a particle size ≤40 μm. SiOC/C with very low content of segregated carbon (<1 vol.%) was synthesized from polysiloxane microspheres (Tospearl 2000B) upon pyrolysis in hydrogen atmosphere, as described previously.[26),27)] Both powders were hot-pressed at 1400 and 1600°C (50 MPa, Argon atmosphere, 30 min) to obtain monolithic samples. Diamond nanoparticles (particle size ≤10

† Corresponding author: E. Ionescu; E-mail: ionescu@materials.tu-darmstadt.de
†† Corresponding author: N. Nicoloso; E-mail: nicoloso@materials.tu-darmstadt.de
††† Preface for this article: DOI http://dx.doi.org/10.2109/jcersj2.124.P10-1

DOI http://dx.doi.org/10.2109/jcersj2.16100

nm, Sigma-Aldrich) and β-silicon carbide (β-SiC, particle size $\leq$400 nm, Sigma-Aldrich) were used as reference materials.

A tunable Ti:sapphire solid state laser (Coherent, Indigo-S) with an excitation wavelength of 256.7 nm (i.e., 4.8 eV) was employed for the UV Raman studies carried out at room temperature. Anisotropic BBO (β-barium borate) and LBO (lithium triborate) crystals have been used to generate the UV radiation by frequency tripling the fundamental (770.1 nm) of the laser. Scattered radiation is dispersed and detected with a triple stage spectrometer (Princeton Instruments, TriVista 555) equipped with a CCD camera (Princeton Instruments, Spec10:2kBUV). The spectral resolution of the spectrometer is $\approx$1 cm^{-1}. For a more detailed description of the laser assembly and the spectrometer, the reader is referred to Ref. 28.

A mirror system has been designed to guarantee an efficient collection of the scattered Raman photons. A spherical mirror (Edmund Optics) focuses the laser beam onto the sample. Two 90° off-axis parabolic mirrors (Thorlabs) collect and refocus the scattered photons into the spectrometer.

Prior to each measurement, the spectrometer has been calibrated using boron nitride (BN, 99%) and the laser power was reduced to $\leq$400 µW to avoid sample damage. The acquisition time of each spectrum was $\geq$1 h to obtain a signal-to-noise ratio $\geq$3. All spectra were background subtracted, smoothed (SMA, simple moving average) using Matlab R2010a and fitted to Lorentzian line shapes using Origin Pro 9.1.0G.

3. Results and discussion

Figure 1 compares the UV Raman spectrum of SiOC/C ($\leq$1 vol.%) prepared upon pyrolysis at 1100°C with those of diamond nanoparticles ($\leq$10 nm), highly ordered pyrolytic graphite (HOPG) and of β-SiC. Nanodiamond and SiC show the characteristic modes of sp^3-bonded tetrahedral carbon at 1333 cm^{-1} and of the Si–C bond at 790 cm^{-1} (and its 2nd harmonic at 1580 cm^{-1}), respectively. The nanodiamond sample exhibits a broad signal at $\approx$1600 cm^{-1} corresponding to the E_{2g} mode (G band) of polycrystalline surfacial graphite. A much narrower G peak is seen in the spectrum of highly ordererd pyrolytic graphite (HOPG).[29] Note that graphite shows no D mode (1380 cm^{-1}) as it is suppressed in UV Raman.[30] In comparison to these reference materials, the SiOC/C sample does not exhibit the typical resonances of graphitic (or diamond-like) carbon. Therefore, the signals at wave numbers $>$1000 cm^{-1} are considered to belong to non-graphitic carbon. The most prominent feature at 1500 cm^{-1} can be attributed to the E_{2g} mode (G band) in amorphous carbon where conjugated sp^2 bonds (ring- and chain-like structures) coexist with sp^3 single bonds.[31]

According to the elemental analysis,[26] the SiOC/C ($\leq$1 vol.%) sample contains significant amounts of hydrogen ($\approx$24 mol %), suggesting that amorphous hydrogenated carbon (a-C:H) is formed. The band at 1115 cm^{-1} indicates the presence of polyacetylene (–C=C–)$_n$ with chain length n $\approx$ 10.[32] Configurational and conformational deformation leads to the strong broadening of the Raman signal. Short chains (–CH=CH–)$_n$ with n $\leq$ 4 are expected to give rise to a Raman band at $\approx$1650 cm^{-1}. Such a band has been observed only in case of laser excitation with a power $>$1 mW able to fragment the longer chains.

Small polycyclic aromatic hydrocarbons (PAHs) are identified by the signal at 1360 cm^{-1},[32,33] and C–C single bonds (sp^3) by the signal at 980 cm^{-1}.[31] Finally, the broad resonances appearing at 345, 510 and 830 cm^{-1} correspond to glassy $Si_xO_yC_z$ (Si–O, Si–O and Si–C). **Figure 2** depicts the Raman results in the range of 1900–3500 cm^{-1}. All signals can be attributed to the 2nd harmonics of the Raman modes described above. According to Ref. 31 the bands at 3295 and 2940 cm^{-1} correspond to the overtones of polymeric chains (–CH=CH–)$_{n\gg100}$ and of C–H vibrations in a-C:H. The three other bands at 2690, 2390 and 2000 cm^{-1} are overtones of the PAHs, polyacetylene (–CH=CH–)$_{n\approx10}$ and the C–C bonds.

According to the Raman analysis SiOC/C ($\leq$1 vol.%) pyrolyzed at 1100°C in H_2 contains a variety of carbon states determining the actual microstructure. Carbon sp^3- and sp^2-bonds coexist at the local scale creating severe disorder, as displayed by the strong broadening of the Raman signals. There appears to be no formation of larger clusters of either sp^3- or sp^2-type carbon. Especially, we do not see a clear indication of 2-dimensional carbon structures (network of single layer graphene) as proposed in the model description of SiOC/C by Saha et al.[34] and suggested by the etching experiments of SiOC/C with 0.2–31.3 vol.% of segregated carbon.[35] H-terminated edges in PAHs, polyacetylene and a-C:H prevent 2D growth and disorder also favors 3D bonding. Hence, it appears unlikely that the observed carbon structures form a 2D network. The chain and ring structures can act, however, as nucleation centers for extended 3D carbon structures with long-range interaction. Raising the pyrolysis temperature should then result in more ordered/crystalline carbon, i.e. the

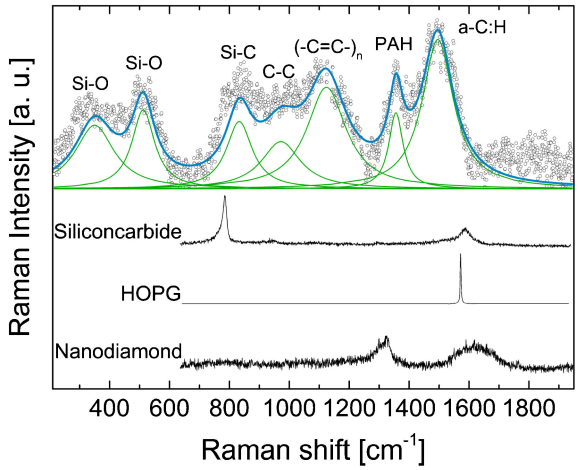

Fig. 1. UV Raman spectra of SiOC/C ($\leq$1 vol.%), SiC, HOPG[29] and nanodiamond. Spectra are offset for clarity.

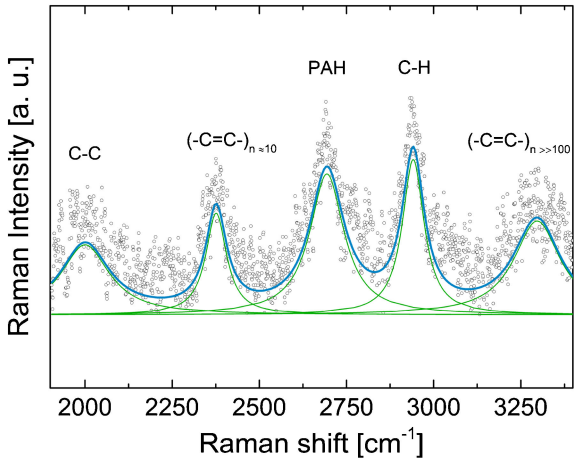

Fig. 2. UV Raman spectrum of SiOC/C ($\leq$1 vol.% of segregated carbon) within the range of 1950–3300 cm^{-1}.

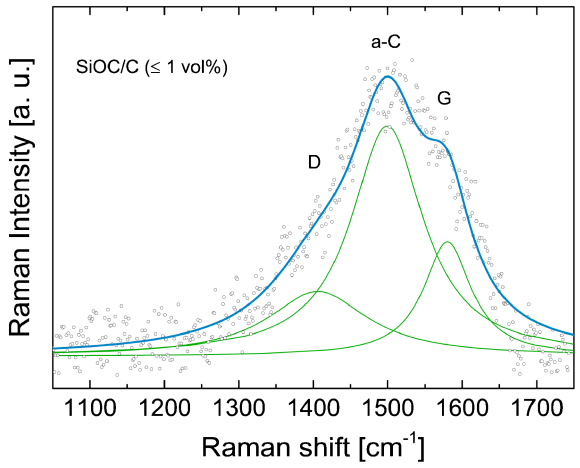

Fig. 3. UV Raman spectra of the SiOC/C sample with ≤1 vol.% of segregated carbon pyrolyzed at 1400°C.

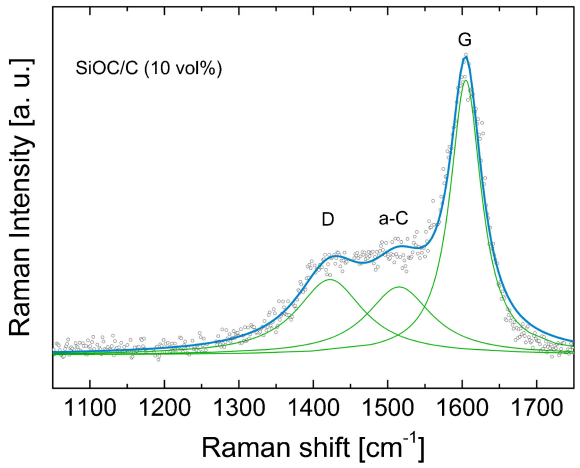

Fig. 4. UV Raman spectra of the SiOC/C sample with 10 vol.% of segregated carbon pyrolyzed at 1400°C.

concentration of olefinic chains, PAHs and a-C:H should decline at the expense of nanocrystalline graphite. Accordingly, the Raman spectrum at $T \gg 1000°C$ should be dominated by the G and D band of graphite-like carbon. As shown in **Fig. 3**, the polyacetylene and polycyclic aromatic hydrocarbon bonds have disappeared and only a broad resonance at 1500 cm^{-1} with shoulders at 1600 and 1380 cm^{-1} is visible in the SiOC/C sample (≤1 vol.%) pyrolyzed at 1400°C.

The deconvolution of the spectrum clearly demonstrates the occurrence of polycrystalline graphite (G and D band at 1600 and 1380 cm^{-1}, respectively) besides amorphous carbon.

As supported by elemental analysis,[26] the change in the carbon microstructure results from the loss of hydrogen at temperatures in the range of 1000 to 1250°C: breaking up C–H bonds promotes the formation of aromatic sp^2-bonded carbon. Note that under the chosen experimental conditions amorphous carbon still exists, indicating an early stage of graphitization.

Figure 4 shows the UV Raman spectrum of the SiOC/C (10 vol.%) sample processed under the same conditions as the SiOC/C (≤1 vol.%) sample, but starting from a different precursor. Comparison of Figs. 3 and 4 allows to estimate the impact of the precursor on the graphitization process. Both samples show the same carbon signals, i.e. D (≈1400 cm^{-1}), a-C (≈1500 cm^{-1}) and G (≈1600 cm^{-1}) but with different relative intensities. The change in the signal intensities as well as the shift of the G-band from 1580 cm^{-1} (SiOC/C ≤ 1 vol.%) to 1600 cm^{-1} (SiOC/C = 10 vol.%) signalize the (gradual) change from amorphous to nanocrystalline carbon.[13] The graphitization progresses at different rates in the two samples, as indicated by the decrease of the intensity of the a-C signal with respect to the G-band, i.e. the formation of graphitic domains proceeds faster in the carbon-rich sample. The transformation to nanocrystalline carbon can be regarded as finished when the a-C signal disappears. **Figure 5** presents the UV Raman spectrum of the SiOC/C sample with 10 vol.% segregated carbon pyrolyzed and hot-pressed at 1600°C under Argon. The band due to a-C has vanished and the two characteristic UV Raman bands of graphitic carbon appear: the G band at 1580 cm^{-1} and the complex signal at ≈3000 cm^{-1} due to double resonant Raman scattering.[36),37] The inset of Fig. 5 displays the deconvolution of the latter signal.

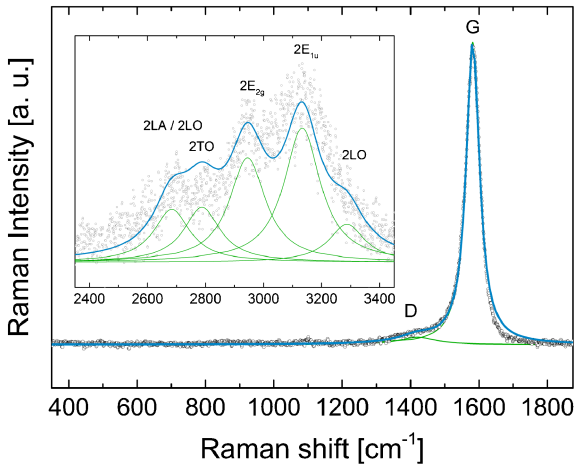

Fig. 5. UV Raman spectrum of SiOC/C (10 vol.% segregated carbon/1600°C). The inset presents the Raman modes due to double resonant scattering.

The peak positions of the fitted lines are in excellent agreement with literature UV Raman data for graphite.[38] The only remarkable difference appears to be the broadening of the Raman lines (by a factor of ≈5) which very likely arises from the higher distortion of graphite in contact with the glassy matrix. Note that the obtained data rule out graphene as carbon component in SiOC/C nanocomposites, as assumed in Ref. 35. The UV Raman spectrum of single layer graphene shows less marked signal structure, i.e. fewer peaks are observed in the range of 2600 to 3400 cm^{-1}.[38] The weak but still visible D peak and the change in the full width at half maximum (FWHM) of the G signal also hint at non-ideal graphite. The FWHM exceeds the value of highly-ordered graphite by far ($FWHM_{HOPG} = 10\ cm^{-1}$) and decreases only slightly from 51 cm^{-1} (1400°C) to 47 cm^{-1} (1600°C). The lateral size L_a of non-distorted/ideally crystallized graphite can be estimated from Raman measurements with visible light (514 nm) yielding domain sizes of ≤2 nm, which remain almost constant within the temperature range 1400–1600°C.[39] Combining these data with our UV Raman results, the state of carbon or stage of graphitization at T = 1600°C, respectively, can be best described by turbostratic carbon.

4. Summary and conclusion

SiOC/C ceramics with two different concentrations of segregated carbon (≤1 and 10 vol.%) processed at temperatures

1100°C < T < 1600°C have been investigated by UV Raman spectroscopy ($\lambda = 256.7$ nm) to follow the different stages of the graphitization of the carbon phase. At 1100°C, carbon forms a non-uniform amorphous sp^2–sp^3 bonded network in SiOC/C (≤1 vol.%) including C–C single bonds, polymeric chains and small polycyclic aromatic hydrocarbons. Dehydrogenation at about 1200°C promotes sp^2 bonding at the expense of sp^3 bonding creating extended aromatic carbon structures. The transformation of amorphous carbon to nanocrystalline carbon at T > 1400°C is seen in the Raman spectra of SiOC/C (≤1 vol.%) and SiOC/C (10 vol.%) by the decrease of the a-C signal and the appearance of the G band (and its shift to higher wavenumbers) of crystalline carbon. Upon thermal annealing at 1400°C < T < 1600°C, the nanocrystalline carbon phase gradually transforms into graphite which is, however, far from being well-ordered at T = 1600°C. In agreement with previous TEM studies,[40] the obtained results suggest the presence of turbostratic carbon within the SiOC glassy matrix and do not support the model description of carbon as a network of single layer graphene bonded to silica SiO_mC_{4-m} tetrahedra (1 < m < 4).

Acknowledgement The authors thank R. Riedel for his continuous support. Financial support by the Deutsche Forschungsgemeinschaft (DFG, Ri 510/52-1 and INST, 163/130-1 FUGG) is gratefully acknowledged.

References

1) E. Ionescu, B. Papendorf, H.-J. Kleebe and R. Riedel, *J. Am. Ceram. Soc.*, **1789**, 1783–1789 (2010).
2) E. Ionescu, B. Papendorf, H.-J. Kleebe, F. Poli, K. Müller and R. Riedel, *J. Am. Ceram. Soc.*, **93**, 241–250 (2010).
3) A. Saha and R. Raj, *J. Am. Ceram. Soc.*, **90**, 578–583 (2007).
4) B. Papendorf, E. Ionescu, H.-J. Kleebe, C. Linck, O. Guillon, K. Nonnenmacher and R. Riedel, *J. Am. Ceram. Soc.*, **96**, 272–280 (2013).
5) C. Stabler, F. Roth, M. Narisawa, D. Schliephake, M. Heilmaier, S. Lauterbach, H.-J. Kleebe, R. Riedel and E. Ionescu, *J. Eur. Ceram. Soc.*, **36**, 3747–3753 (2016).
6) L. Toma, H.-J. Kleebe, M. M. Müller, E. Janssen, R. Riedel, T. Melz and H. Hanselka, *J. Am. Ceram. Soc.*, **95**, 1056–1061 (2012).
7) M. Graczyk-Zajac, L. Reinold, J. Kaspar, P. Sasikumar, G.-D. Soraru and R. Riedel, *Nanomaterials (Basel)*, **5**, 233–245 (2015).
8) Q. Wen, Y. Feng, Z. Yu, D.-L. Peng, N. Nicoloso, E. Ionescu and R. Riedel, *J. Am. Ceram. Soc.*, **99**, 2655–2663 (2016).
9) G. Mera, I. Menapace, S. J. Widgeon, S. Sen and R. Riedel, *Appl. Organomet. Chem.*, **27**, 630–638 (2013).
10) L. Bois, J. Maquet, F. Babonneau and D. Bahloul, *Chem. Mater.*, **7**, 975–981 (1995).
11) G. Das, P. Bettotti, L. Ferraioli, R. Raj, G. Mariotto, L. Pavesi and G. D. Sorarù, *Vib. Spectrosc.*, **45**, 61–68 (2007).
12) M. Monthioux and O. Delverdier, *J. Eur. Ceram. Soc.*, **16**, 721–737 (1996).
13) A. C. Ferrari and J. Robertson, *Phys. Rev. B*, **61**, 14095–14107 (2000).
14) J. Schwan, S. Ulrich, V. Batori, H. Ehrhardt and S. R. P. Silva, *J. Appl. Phys.*, **80**, 440–447 (1996).
15) J.-P. Tessonnier, D. Rosenthal, T. W. Hansen, C. Hess, M. E. Schuster, M. R. Blume, F. Girgsdies, N. Pfänder, O. Timpe, D. S. Su and R. Schlögl, *Carbon*, **47**, 1779–1798 (2009).
16) M. S. Dresselhaus, G. Dresselhaus, A. Jorio, A. G. Souza Filho and R. Saito, *Carbon*, **40**, 2043–2061 (2002).
17) M. S. Dresselhaus, G. Dresselhaus, R. Saito and A. Jorio, *Phys. Rep.*, **409**, 47–99 (2005).
18) L. M. Malard, M. A. Pimenta, G. Dresselhaus and M. S. Dresselhaus, *Phys. Rep.*, **473**, 51–87 (2009).
19) A. C. Ferrari and D. M. Basko, *Nat. Nanotechnol.*, **8**, 235–246 (2013).
20) A. C. Ferrari, *Solid State Commun.*, **143**, 47–57 (2007).
21) F. Tuinstra and J. L. Koenig, *J. Chem. Phys.*, **53**, 1126–1130 (1970).
22) A. C. Ferrari, S. E. Rodil, J. Robertson and W. I. Milne, *Diamond Relat. Mater.*, **11**, 994–999 (2002).
23) G. Irmer and A. Dorner-Reisel, *Adv. Eng. Mater.*, **7**, 694–705 (2005).
24) S. R. Sails, D. J. Gardiner, M. Bowden, J. Savage and D. Rodway, *Diamond Relat. Mater.*, **5**, 589–591 (1996).
25) N. Wada, P. J. Gaczi and S. A. Solin, *J. Non-Cryst. Solids*, **35–36**, 543–548 (1980).
26) M. Narisawa, S. Watase, K. Matsukawa, T. Dohmaru and K. Okamura, *Bull. Chem. Soc. Jpn.*, **85**, 724–726 (2012).
27) M. Narisawa, S. Watase, K. Matsukawa, T. Kawai, Y. Kawamoto, T. Matsui and A. Iwase, *J. Non-Cryst. Solids*, **391**, 1–5 (2014).
28) D. Nitsche and D. C. Hess, *J. Raman Spectrosc.*, **44**, 1733–1738 (2013).
29) R. W. Bormett, S. A. Asher, R. E. Witowski, W. D. Partlow, R. Lizewski and F. Pettit, *J. Appl. Phys.*, **77**, 5916–5923 (1995).
30) V. N. Mochalin, O. Shenderova, D. Ho and Y. Gogotsi, *Nat. Nanotechnol.*, **7**, 11–23 (2012).
31) A. C. Ferrari and J. Robertson, *Philos. Trans. A. Math. Phys. Eng. Sci.*, **362**, 2477–2512 (2004).
32) C. Castiglioni, M. Tommasini and G. Zerbi, *Philos. Trans. A. Math. Phys. Eng. Sci.*, **362**, 2425–2459 (2004).
33) M. Signorile, F. Bonino, A. Damin and S. Bordiga, *J. Phys. Chem. C*, **119**, 11694–11698 (2015).
34) A. Saha, R. Raj and D. L. Williamson, *J. Am. Ceram. Soc.*, **89**, 2188–2195 (2006).
35) R. Pena-Alonso, G. D. Soraru and R. Raj, *J. Am. Ceram. Soc.*, **89**, 2473–2480 (2006).
36) C. Thomsen and S. Reich, *Phys. Rev. Lett.*, **85**, 5214–5217 (2000).
37) S. Reich and C. Thomsen, *Philos. Trans.*, **362**, 2271–2288 (2004).
38) C. Tyborski, F. Herziger, R. Gillen and J. Maultzsch, *Phys. Rev. B*, **92**, 041401 (2015).
39) F. Roth, C. Schmerbauch, E. Ionescu, N. Nicoloso, O. Guillon and R. Riedel, *J. Sensors Sens. Syst.*, **4**, 133–136 (2015).
40) H.-J. Kleebe, G. Gregori, F. Babonneau, Y. D. Blum, D. B. MacQueen and S. Masse, *Zeitschrift für Met.*, **97**, 699–709 (2006).